

Received: 23 September 2017 / Accepted: 08 December 2017 / Published online: 20 December 2017

*sculptured surfaces, 5-axis milling,  
cutting layer, cutting forces  
toroidal cutter*

Michał GDULA<sup>1\*</sup>

Jan BUREK<sup>1</sup>

## **CUTTING LAYER AND CUTTING FORCES IN A 5-AXIS MILLING OF SCULPTURED SURFACES USING THE TOROIDAL CUTTER**

The purpose of this article was to evaluate the significance of the influence of five-axis orientation parameters of a toroidal cutter axis and the geometrical parameters of the machined sculptured surface on the intersection of the cut layer in a 5-axis machining. An impact assessment was performed by simulating concave-convex and convex-concave surfaces using a discrete method of direct transformation in a CAD environment. It was shown that only the radius of curvature of the surface in the feed direction and the angle of the tool axis affected the change in the intersection of the cutting layer. Subsequently, experimental tests were conducted that aimed at determining the mathematical models of the influence of these important parameters on the components of the cutting force. The object of the experimental studies was a convex and concave surface of a turbine blade of Inconel 718 alloy. The R300-016B20L-08L Sandvik Coromant toroid cutter was used for the tests. Based on the results of the study it was found that the lead angle in the machining of the convex surface and concave turbine blade should be continuously varied with the change of radius of curvature in the direction of the machined surface profile.

### **1. INTRODUCTION**

5-axis milling technologies are now commonly used to produce geometrically sophisticated parts for the aviation industry, among them there are molds and matrices both automotive as well as biomedical ones. By combining three linear and two additional rotational movements the 5-axis milling process allows the tool to move in space continuously with respect to the vector of the normal workpiece. Thanks to this geometric complex shapes can be machined in one attachment, thus reducing the total time of parts production. In addition, the kinematic freedom of 5-axis machining allows to increase the availability of the tool while reducing its reach. The use of a shorter tool with the right geometry for the 5-axis machining not only makes the machine tool-holder-tool-object system more rigid, but also delivers high quality surfaces and increases its productivity.

---

<sup>1</sup> The Rzeszow University of Technology, Department of Manufacturing Techniques and Automation, 2 W. Pola Street, 35-959, Rzeszow, Poland

\* E-mail: gdulam@prz.edu.pl

DOI: 10.5604/01.3001.0010.7009

For this reason, toroidal cutters are increasingly used in industrial practice for the 5-axis machining of composite surfaces [1].

In addition to reducing machining time, the main purpose of the 5-axis milling process is to increase geometric accuracy of workpieces. This cannot be achieved satisfactorily without deriving model relationships that describe the relations between the geometric parameters of the sculptured surface and the kinematic orientation of the toroidal milling axis. It should be borne in mind that the change in the value of the cross-sectional area of the cut layer results from the continuous change of its curvature, and as a result of the change in the value and direction of the cutting forces, resulting in dimensional inaccuracy. Therefore, the definition of model relationships between the parameters of the tool axis orientation and the curvatures of the machined surface and the components of the cutting force becomes more significant in order to increase the accuracy of the 5-axis machining.

Most 5-axis machining research focuses on aspects of this process in CAM systems such as: toolpaths generation, toolpaths optimization, and geometric toolpaths verification. The improvement of CAM technology in such a case eliminates some geometrical constraints and errors in the program itself. By contrast, by refining the CAM systems, the geometrical and kinematic aspects of the 5-axis milling process that have occurred in the cutting zone have not been taken into account.

Fussell et al. [2] have developed a virtual 5-axis machining environment that enables a discrete simulation of sculptured machined surfaces to automatically select the feed along the toolpath using a mechanistic model of the cutting force component. In turn, Bailey et al. [3] proposed in this paper a method of process optimization that is based on the use of the feed rate value calculated from the maximum cutting thickness and cutting force, which are constraints.

One of the latest research in the area of 5-axis milling was carried out by Ozturk, Budak et al. [4-6] and Erdim and Lazoglu et al. [7,8]. These studies concerned an analytical modeling of the cut layer geometry and they obtained data that were later used to predict the cutting force and optimize the 5-axis milling process. Ferry and Altintas in their work [9] described a developed virtual machining simulation system for 5-axis flank milling of jet engines.

One of the main problems in 5-axis milling is the positioning of the cutter axis in relation to the machined surfaces normal vector in the CAM systems in order to machine without having overcut or undercut. In order to avoid these problems, a specified lead or/and tilt angle can be used, instead of perpendicular cutting conditions. Overcutting does not cause a big problem when using ball-end cutters. However, this method is only advantageous for machining highly curved surfaces. To machine low-curvature surfaces, for example the turbine blade surfaces, a toroidal cutter is more advantageous. Simultaneous 5-axis milling of the toroidal cutter enables a smaller number of cutting passes to be used and as a result a shorter machining time is needed [1,10-11]. Because of this, this study focuses on milling using a toroidal cutter. Additionally, when 5-axis milling is used to machine a sculptured surface with toroidal cutter, the tool orientation can be controlled by either a lead or a tilt angle. Actually, since the cut geometry with ball-end cutters always occurs on a spherical cap, the cut geometry does not vary as a function of tool axis

orientation in 5-axis milling. The influences of the tool axis orientation on the engagement parameters when using ball-end cutters have been investigated [4-6,12-14], but this effect has not been investigated using a toroidal cutter [10],[15,16].

## 2. 5-AXIS MILLING OF SCULPTURED SURFACES

### 2.1. VARIABLE OF 5-AXIS MILLING PROCESS

Sculptured surfaces are used to describe complex convex, concave, biconvex, biconcave, convex or convex-concave shapes. The sculptured surface is generally curved in both the major parametric directions  $u$  and  $v$ . The final surface shape is characterized by the values of the principal curvatures in the vicinity of the selected point  $P$  on that surface. The principal curvatures in this paper were geometric variables of the surface in the 5-axis milling process and were considered as  $\rho_1$  and  $\rho_2$ , as shown in Fig. 1.

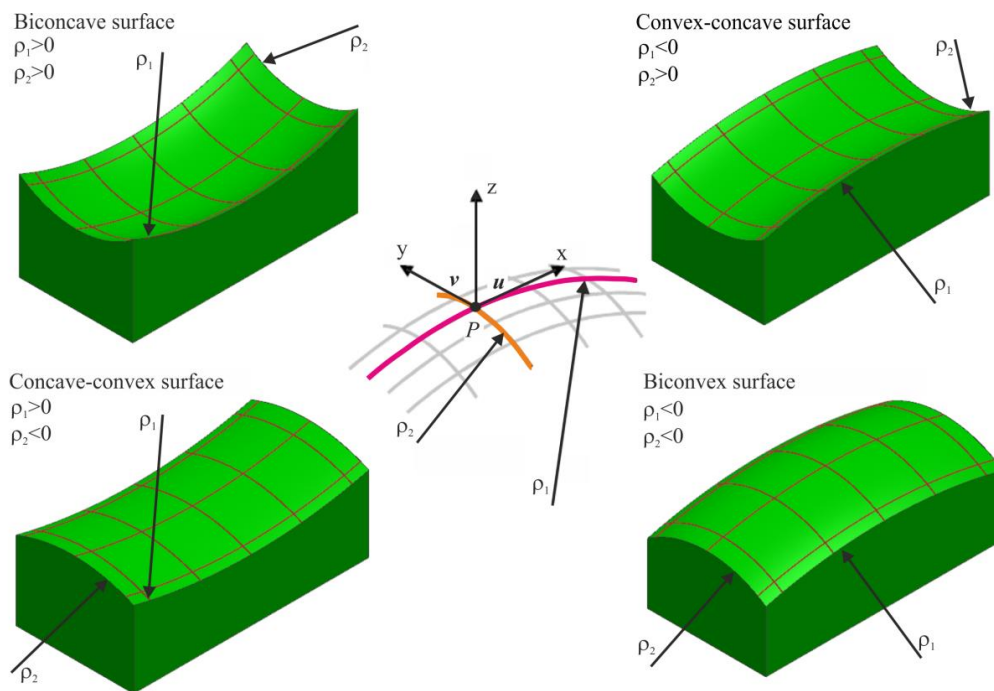


Fig. 1. Geometric parameters of sculptured surfaces as variable 5-axis milling [1]

One of the main problems of 5-axis milling is to select the optimal orientation of the toroidal milling cutter relative to the normal surface vector. The orientation of the cutter axis is defined by programming the kinematical parameters of the lead angle  $\alpha$  and/or inclination angle  $\beta$ , as schematically shown in Fig. 2. These parameters determine uniquely the conditions and the contact area between the cutting edge and the work surface and are crucial for the final cutting result [12,15]. The kinematic parameters of 5-axis milling were used in the present work as further variables of the analyzed surface machining process.

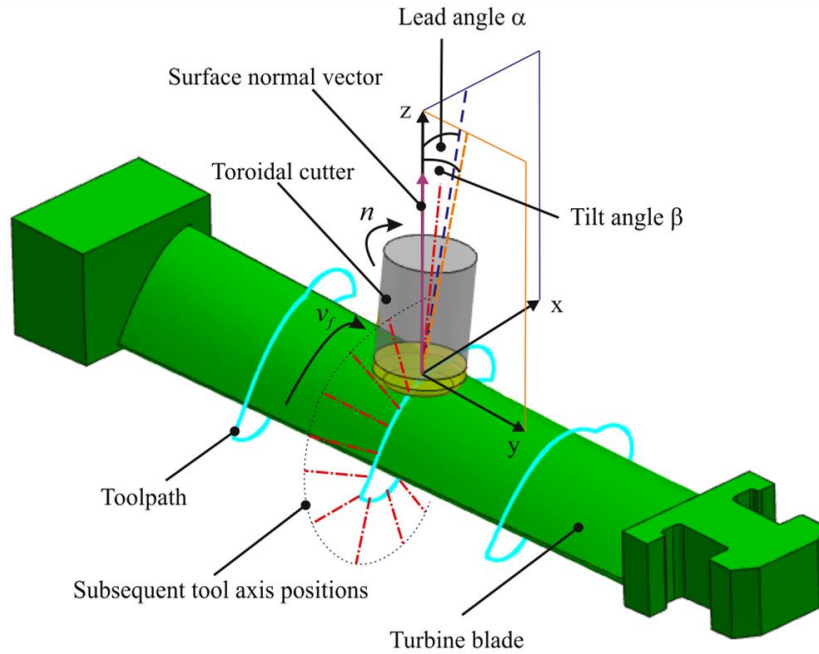


Fig. 2. Kinematic parameters of 5-axis milling as process variables [1]

## 2.2. PARAMETERS OF 5-AXIS MILLING PROCESS

### 2.2.1. CUT LAYER

Geometry of the cut layer in the machining with the use of toroidal (or ball-end mill) cutter has a distinctive “comma” shape, and the thickness of the cut layer  $h$  is shifted along the active cutting edge  $b$ , as schematically shown in Fig. 3. In the machining of the toroidal cutter the geometry of the cut layer is influenced by the radius of the circular cutting plate  $r_p$ , feed rate on the cutter blade  $f_z$ , and the axial feed  $a_p$ . [1,10].

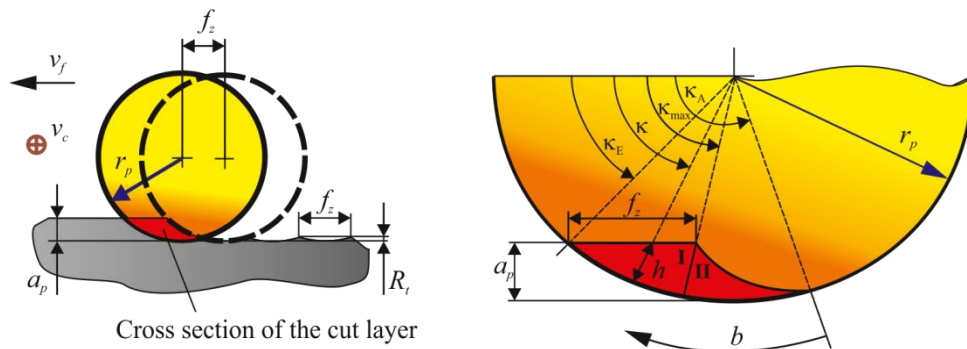


Fig. 3. Geometry of the cut layer [18]

In the mathematical description of the cross sectional geometry of the cut layer, two areas can be distinguished – I and II, as shown in Fig. 3. Within the boundaries of the zones I and II of the cross section of the cut layer, the author of work [17] has

introduced the angle  $\kappa$  at the individual boundary points. The uncut chip thickness  $h$  at any point of the cross sectional area of cut in relation to the angle  $\kappa$  can be evaluated from the relationship:

$$h_1(\kappa) = r_p - \left( \frac{r_p - a_p}{\sin(\kappa)} \right) \quad (1)$$

where:  $h_1$  – chip thickness in area I,

$$h_2(\kappa) = r_p + f_z \cdot \cos(\kappa) - \sqrt{r_p^2 - f_z^2 \cdot \sin(\kappa)^2} \quad (2)$$

where:  $h_2$  – chip thickness in area II.

In the 5-axis milling process the variation of the geometric parameters of the cut layer in time is also significant and it is caused by [12,16,17,19]:

- process kinematics, i.e. the angular parameters of the tool axis orientation,
- surface geometry, i.e. variable radii of the machined surface curvature.

In previous research works no attempt was made to determine the significance of the influence of variable radii of the sculptured surface curvature and kinematic parameters of 5-axis machining while maintaining constant geometry of toroidal cutter and constant milling technological parameters on the formation of the cut layer section.

### 2.2.2. CUTTING FORCES

The total force exerted by the tool on the workpiece is defined as the resultant of the cutting forces exerted by all the tool cutting blades [6,11,15,19,20]. The components of the total force are determined by the rectangular projection of this force along the direction of the individual motions associated with the kinematics of the cutting process. For the 5-axis milling with a toroidal cutter the authors [15] give the following distribution of forces, as shown in Fig. 4. This distribution is due to Altintas-Lee cutting force model.

According to this model, the total cutting force generated in the milling process with the toroidal cutter (or spiral cutter) can be broken down into three components in the tool system acting on the cross sectional area of the cut layer as a function of the angular position of the milling cutter. These components are: tangential force  $F_t(\varphi)$ , radial force  $F_r(\varphi)$  and axial force  $F_a(\varphi)$ .

The components of total force can be expressed by the following equation:

$$\begin{aligned} F_t(\varphi) &= K_{tc}A(\varphi) + K_{te}b \\ F_r(\varphi) &= K_{rc}A(\varphi) + K_{re}b \\ F_a(\varphi) &= K_{ac}A(\varphi) + K_{ae}b \end{aligned} \quad (3)$$

where:  $K_{tc}$ ,  $K_{rc}$ ,  $K_{ac}$  – coefficients of specific cutting resistance depending on the cross-sectional area of the cutting layer  $A(\varphi)$ ,  $K_{te}$ ,  $K_{ae}$ ,  $K_{re}$  – coefficients of the specific cutting resistance depending on the active cutting edge length  $b$ .

The basic component of dependence (3) is the momentary cross-sectional area of the cutting layer  $A(\varphi)$ , which describes the relationship:

$$A(\varphi) = \frac{a_p f_z \sin(\varphi)}{\sin \kappa_r} \quad (4)$$

where:  $a_p$  - axial infeed,  $f_z$  – feed rate on the blade,  $\varphi$  - momentary angle of blade position,  $\kappa_r$  – tool cutting edge angle.

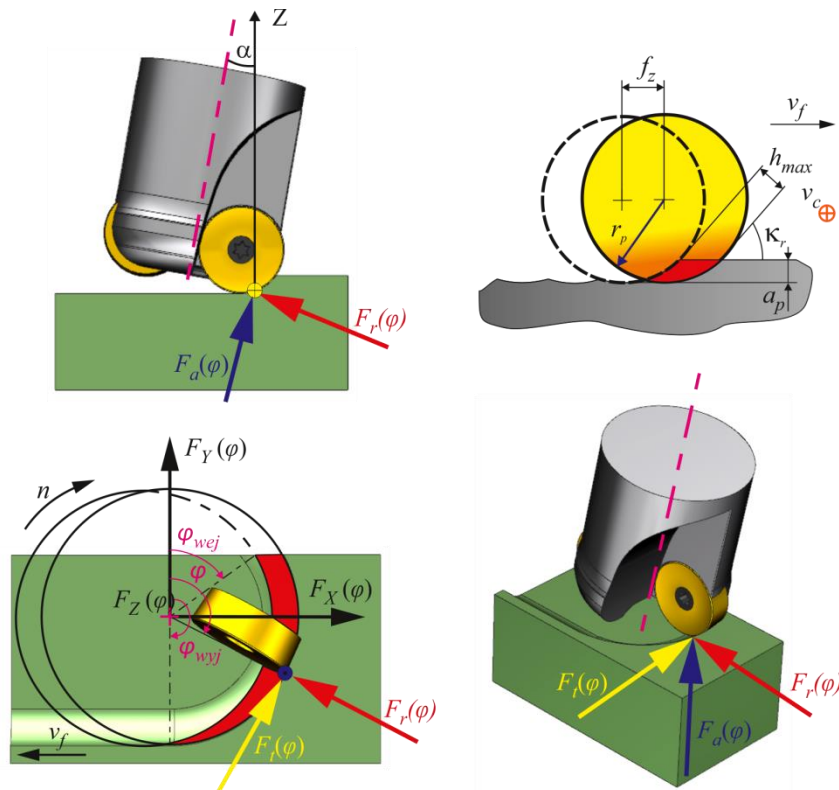


Fig. 4. Distribution of forces at 5-axis milling with a toroidal cutter [1]

From dependencies (3) and (4) it follows that the cutting force component values depend on the geometry of the cutting section, mainly affected by axial infeed  $a_p$ , feed rate on blade  $f_z$ , angle of cutter milling cutter angle  $\varphi$  and  $\kappa_r$  – tool cutting edge angle. As shown in the work [21] the tool cutting edge angle  $\kappa_r$  has a major influence on the geometry of the cutting layer and the machining power generated in the machining process. As a result of the variable radii of curvature of the surface to be treated, there is a change in the  $\kappa_r$  between the cutting edge of the cutter blade and the work surface. A continuous change of the tool cutting edge angle  $\kappa_r$ , even with steady cutting parameters: axial infeed  $a_p$ , radial infeed  $a_e$ , feed  $f$  and tool rotational speed  $n$  makes the constant change of the contact point of the cutter blade with the surface to be machined, and thus the change of the cross section of the cutting layer. Hence, changes in these values may result in changes in the value and direction of the radial component  $F_r(\varphi)$ , tangent  $F_t(\varphi)$  and axial  $F_a(\varphi)$  the cutting force. This leads in turn to the variable deformation of the resilient tool and the workpiece, which greatly influences the accuracy of the shape.

Hence, the range of work described in the first part of this article included the simulation of the 5-axial milling of the convex-concave and concave-convex surfaces in order to evaluate the significance of the curvature radii  $\rho_1$  and  $\rho_2$  these surfaces and the angle of inclination  $\alpha$  and/or inclination  $\beta$  of toroidal milling cutter axis. In the second stage experimental studies were carried out. It was based on previous simulation studies parameters of the tool axis orientation and radius of curvature of the surface to determine the model dependencies of these parameters on the value of the cutting force components in the assumed range of tested variables.

### 3. SIMULATION TESTS

For simulation tests the method of a tool direct transformation in a CAD environment was applied, which was used among others in [1,4,6]. This method is based on mathematical models of solids used in CAD/CAM systems. The workpiece and tool were modeled in a solid way, which enabled Boolean operations on these bodies to be performed.

The simulation consisted of discretely changing the positioning of the workpiece and the toroidal cutter with the motions according to kinematics of the 5-axis machining.

In each discrete position, the common part of the bodies representing the perpendicular and the workpiece was a sliced layer.

Because logical operations are performed in a purely geometric manner, the simulation does not take into account such phenomena as the elastic deformations of the machine tool-holder-tool-object system, vibration, temperature, etc. that are present in the actual machining process.

#### 3.1. METHODOLOGY OF SIMULATION TESTS

In the adopted simulation methodology the interference of the workpiece and tool was determined in each successive discrete position of the tool. In this case it was necessary to perform two Boolean operations: product and subtraction. The tool model was placed at a specific location in the CAD work space and copied to each other discrete location from this location. Copying a tool from a fixed place in space eliminates the numerical error associated with logical operations.

The 3D model of the toroidal cutter, which is shown in Fig. 5, is based on its operating surface. Operation surface is the one where the cutting edges of the milling cutter make a circle in the space as a result of the main movement around the axis of the milling head of the milling machine. The cutter moved relative to the workpiece with the motions that resulted from the actual spindle feed kinematics with a fixed step. In the case under consideration this movement was consistent with the velocity vector  $v_f$ , while the discretization step, i.e. the change of the mutual position of the work surface of the cutter and the workpiece was equal to the feed rate value on the blade  $f_z$ . The solid models of the analyzed surfaces are shown in Fig. 6.

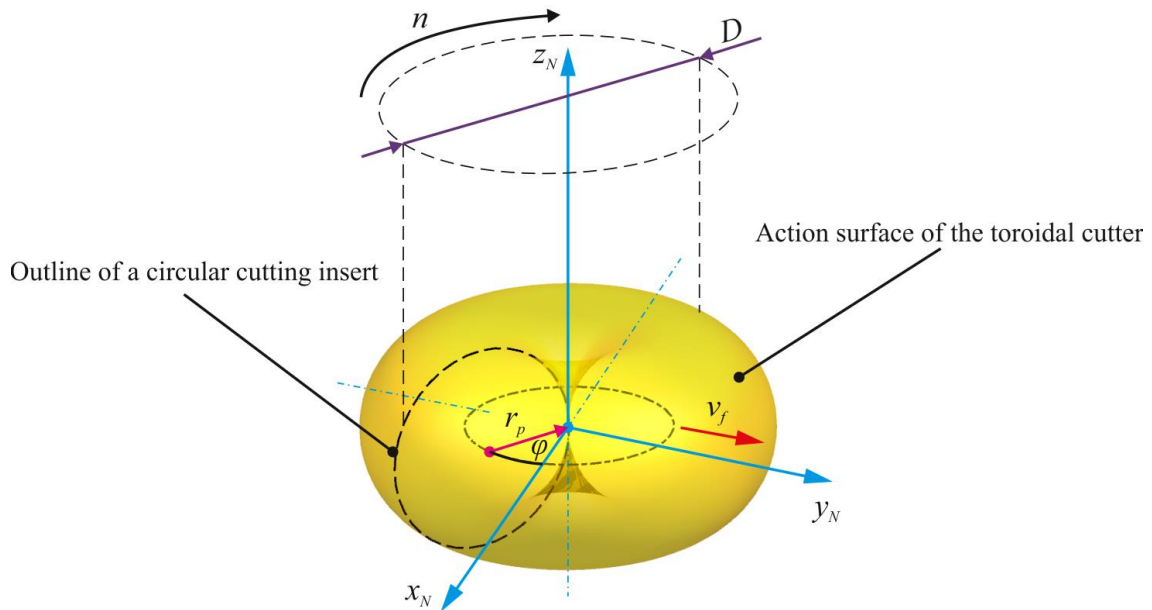


Fig. 5. Toroid milling model formed on the basis of the surface work

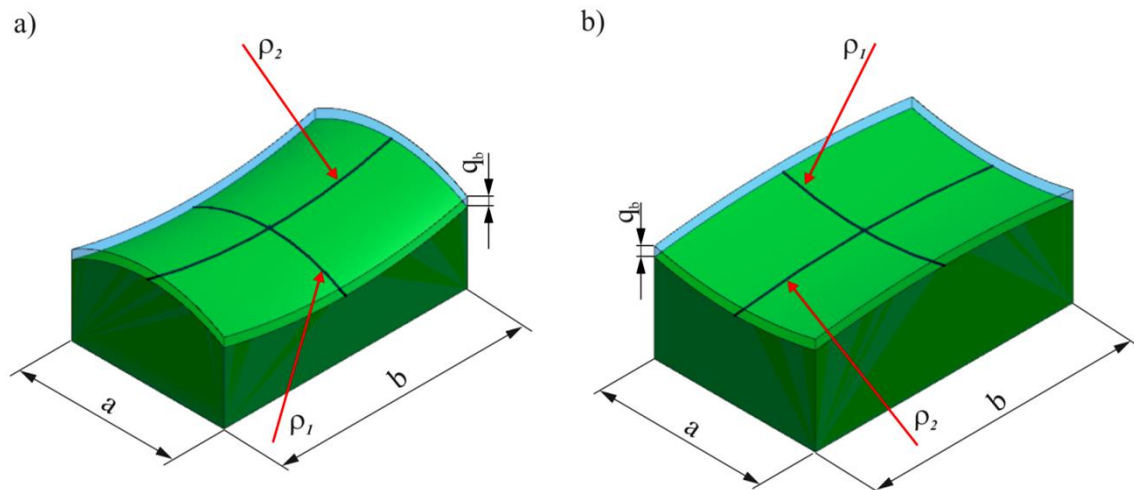


Fig. 6. 3D models of the analyzed surfaces: a) convex-concave, b) concave-convex

They were formed as an output semi-finished products with an assumed allowance  $q_b$ . The geometry of these models was obtained by directly simulating the CAD projection of the surface of the toroidal cutter. 3D models were used for simulations which corresponded to rectangular cubes with dimensions of  $a$  and  $b$  limited respectively by convex-concave and concave-convex surface with curved radii in the feed direction  $\rho_1$  and in the direction perpendicular to the feed direction  $\rho_2$ .

The accepted simulation machining system is shown in Fig. 7. Finally the output parameter was written, i.e. the total cross-sectional area of the cutting layer on the blade of the toroidal cutter  $A_z$ . Whereas, the characteristic geometry of the cross-section of the cutting layer in the applied CAD model is shown in Fig. 8.

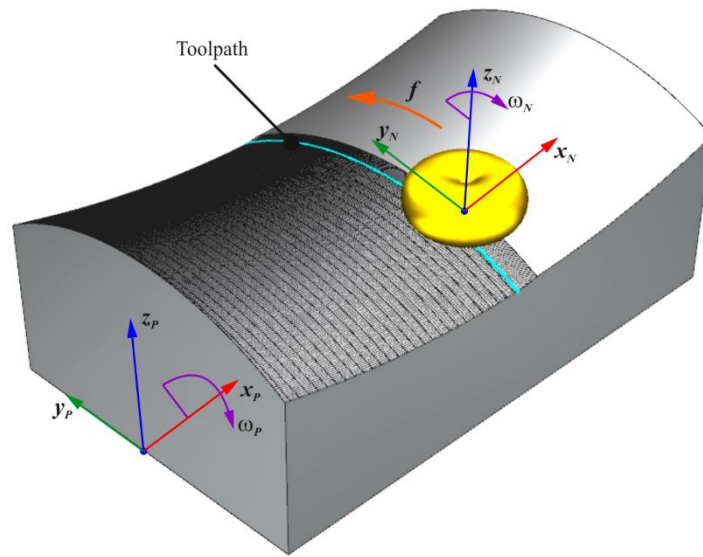


Fig. 7. Accepted machining system in the simulation of machined surface analysis:  $\omega_P$  – angular velocity of the object,  $\omega_N$  - tool angular velocity,  $v_f$  – feed rate velocity,  $S_P(x_P, y_P, z_P)$  – a coordinate system tightly connected with the object,  $S_N(x_N, y_N, z_N)$  - a coordinate system tightly associated with the tool

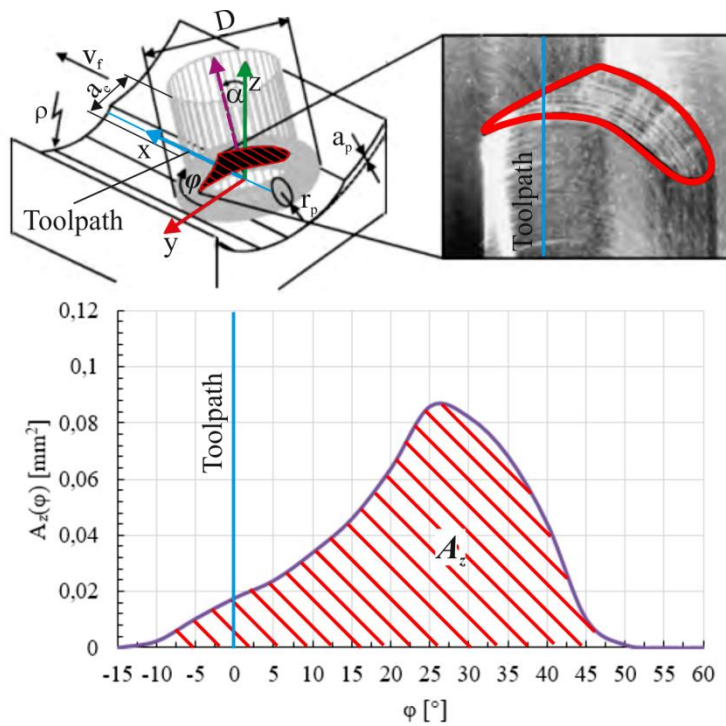


Fig. 8. Characteristic shape of the chip geometry during simultaneous 5-axis milling

### 3.2. CONDITIONS OF SIMULATION TESTS

Simulation tests as described in the following section were carried out with constant technological parameters adopted according to the manufacturer's recommendation of the tool used for the test – R300-016B20L-08L Sandvik Coromant toroidal milling cutter

and object material - nickel alloy Inconel 718. Variable ranges of the machining process which include the angle of inclination  $\alpha$ , the angle of inclination  $\beta$  and radii of curvature  $\rho_1$  and  $\rho_2$  are based on the analysis of the area of adequate tests and are summarized in Table 1. This area was determined on the basis of the different geometries of the turbine blades.

In order to determine the significance of the influence of one or a few inputs on the causative agent, exploratory research was conducted on the basis of a properly selected research program that fulfills certain conditions. The two groups of programs are most often used in impact studies. The first group includes the programs related to variance analysis and these are static programs that are randomized. The applicability of these programs is conditional on the absence of input interactions. The second group is a randomized program – a random balance, which is a randomized (static) program (supersaturated) and Plackett-Burman's (partially saturated) static program.

Due to the presence of four input factors while assuming interaction between them, and that the number of experiments performed in the simulation environment is equal to the number of variables in the model, the simulation study was based on the Plackett-Burman program. The simulation environment was the Siemens NX 10 CAD module.

For each of the steps the fixed parameters were: axial infeed  $a_p$ , radial infeed  $a_e$ , cutting speed  $v_c$ , and feed rate on the  $f_z$  blade. The diameter of the toroidal cutter  $D = 16$  mm and the radius of the circular cutting insert were also constant  $r_p = 4$  mm. Variable parameters within a fixed range were: angle of inclination  $\alpha$ , angle of inclination  $\beta$ , radius of curvature in direction of feed rate  $\rho_1$  and radius of curvature in the direction perpendicular to the feed rate  $\rho_2$ .

Table 1. Conditions of simulation tests

No.	Parameters and variables		Convex-convey surface machining	Convey-convex surface machining
1.	Parameters	$a_p$ [mm]	0.25	0.25
2.		$a_e$ [mm]	1.5	1.5
3.		$f_z$ [mm/blade]	0.14	0,14
4.	Variables	$\rho_1$ [mm]	$\rho_1 \in <25 \div 400>$	$\rho_1 \in <40 \div 120>$
5.		$\rho_2$ [mm]	$\rho_2 \in <800 \div 2000>$	$\rho_2 \in <800 \div 2000>$
6.		$\alpha$ [°]	$\alpha \in <3 \div 18>$	$\alpha \in <7 \div 23>$
7.		$\beta$ [°]	$\beta \in <0 \div 15>$	$\beta \in <0 \div 15>$

### 3.3. RESULTS OF SIMULATION TESTS

#### 3.3.1. DETERMINATION OF THE IMPACT OF THE $\alpha$ , $\beta$ , $\rho_1$ , $\rho_2$ PARAMETERS ON THE INTERSECTION OF THE MACHINED LAYER OF CONVEX-CONCAVE SURFACE

Significance of the influence of the lead angle  $\alpha$ , the angle of inclination  $\beta$ , radius of curvature in the feed direction  $\rho_1$  and the radius of curvature in the direction perpendicular to the feed  $\rho_2$  on the section of the machined layer  $A_z$ , was determined at the assumed significance level of  $\tau=0,05$ . The results obtained on the basis of the simulated

convex-convex surface machining were presented in Table 2. Table 3 shows the calculated significance coefficients in turn for all tested variables. The variance of the experiment was then calculated, the number of degrees of freedom, the  $t$ -Student values were determined and the critical factor of the coefficient of significance  $\tau$  was calculated. For real variables, the values of significance factors were compared with the critical value. This gave the basis for assessing the significance of the influence of the studied variables on the intersection of the machined layer  $A_z$  (Table 4).

Table 2. Total Cross-sectional area of the machined layer  $A_z$  for the assumed levels of variability of parameters  $\alpha$ ,  $\beta$ ,  $\rho_1$ ,  $\rho_2$

	$\beta$ [°]	$\alpha$ [°]	$\rho_1$ [mm]	$\rho_2$ [mm]	$A_z$ [mm <sup>2</sup> ]
1	15	3	400	2000	0.37
2	15	3	25	800	0.67
3	15	18	25	2000	0.25
4	0	18	400	800	0.24
5	15	18	400	800	0.22
6	0	3	400	2000	0.44
7	0	18	25	2000	0.22
8	0	3	25	800	0.38

Table 3. Significance coefficient of the tested variables

	$\beta$ [°]	$\alpha$ [°]	$\rho_1$ [mm]	$\rho_2$ [mm]
$a_i$	0.0288	-0.1163	-0.0463	-0.0438

Table 4. Results of the calculations included in the test plan and an assessment of the significance of the tested variable

Test variance $S_y^2$	0.00036
Standard deviation $S_y$	0.019
Number of degrees of freedom $f$	7
Value of $t$ -Student coefficient $t_{(v,f)}$	2.365
Critical value of coefficient $a_{kr}$	0.0452
Significance assessment $ a_i  > a_{kr}$	
$\beta$ [°]	Insignificant
$\alpha$ [°]	<b>Significant</b>
$\rho_1$ [mm]	<b>Significant</b>
$\rho_2$ [mm]	Insignificant

Based on the obtained results of the simulation and calculations covered by the test plan, it was found that the intersection of the cut layer in 5-axis milling of the convex-concave surface affects only the angle  $\alpha$  and the radius of curvature  $\rho_1$  in the feed direction. The influence of these important parameters, i.e. the lead angle  $\alpha$  and the radius of curvature  $\rho_1$ , on the cross-sectional area of the cutting layer  $A_z$  is shown in Fig. 9.

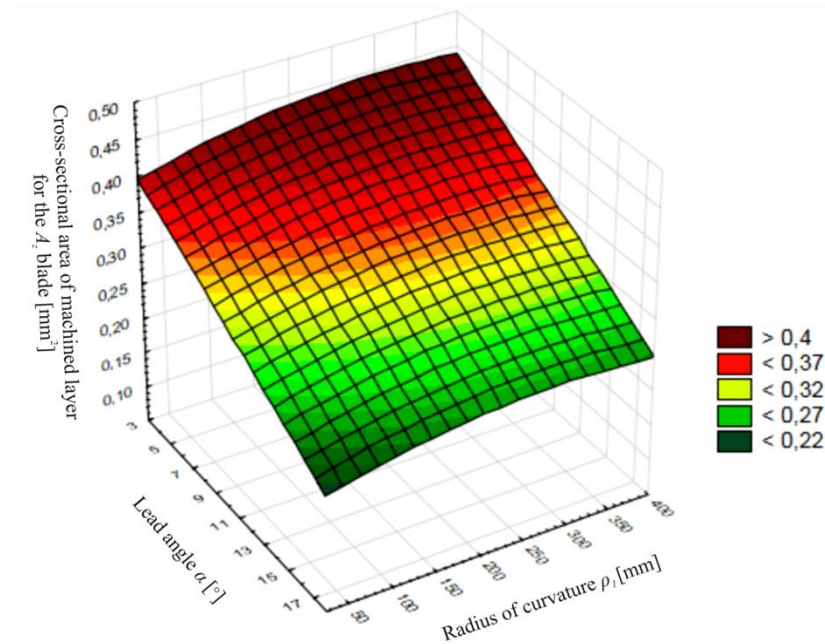


Fig. 9. The impact of the lead angle  $\alpha$  and radius of curvature  $\rho_1$  on total cross-sectional area of machined layer  $A_z$  in the machining of convex-concave surfaces

The diagram shows that the lead angle  $\alpha$  influences much more significantly on the cross-sectional area of the machined layer  $A_z$  than the radius of curvature  $\rho_1$ . An increase of the angle  $\alpha$  from  $3^\circ$  to  $18^\circ$  resulted in a reduction in the cross-sectional area of the cut layer by about 40% for the surface whose workpiece has a radius of  $\rho_1=25$  mm and by about 45% for the contour of the radius  $\rho_1=400$  mm. Increasing the radius of curvature  $\rho_1$  from 25 mm to 400 mm increased the cross-sectional area of the machined layer by about 15% for angle  $\alpha = 3^\circ$  and 10% for angle  $\alpha = 18^\circ$ .

On the other hand, the influence of the inclination angle  $\beta$  and the radius of curvature  $\rho_2$  on the total cross-sectional area of the machined layer  $A_z$  is not significant. Hence, for further experimental studies, the convex-concave surface can be simplified to the convex surface.

### 3.3.2. DETERMINATION OF THE IMPACT OF THE $\alpha$ , $\beta$ , $\rho_1$ , $\rho_2$ PARAMETERS ON THE INTERSECTION OF THE MACHINED LAYER OF CONCAVE-CONVEX SURFACE

The significance of the influence of the lead angle  $\alpha$ , the angle of inclination  $\beta$ , the radius of curvature in the feed direction  $\rho_1$  and the radius of curvature in the direction perpendicular to the feed rate  $\rho_2$  on the intersection of the concave-convex surface are

determined in an analogous manner. The results obtained from the simulation are presented in Table 5. Table 6 summarizes the calculated significance factors for all the variables tested, while the impact assessment is shown in Table 7.

The limitation in the concave-convex surface machining simulation was the value of the minimum lead angle  $\alpha_{min}$  which was calculated from formula 5 for the smallest concave radius of curvature  $\rho_1$  of the machined surface contour in the direction of the tool feed. The value of the parameter  $\alpha_{min}$  was calculated taking into account the geometry of the toroidal cutter used for the test due to the possibility of undercutting of the machined surface.

$$\alpha_{min} = \arcsin \left( \frac{\frac{D}{2} - r_p}{\rho_1 - r_p} \right) \quad (5)$$

where:  $D$ -diameter of the tool,  $r_p$ -radius of the cutting insert,  $\rho_1$ -radius of the concave curvature in the feed direction.

Calculated limit minimum lead angle value that should be applied in the concave-convex surface machining simulation with the selected toroidal cutter was  $\alpha_{min} = 7^\circ$ .

Table 5. Total Cross-sectional area of the machined  $A_z$  layer for the assumed levels of variability of parameters  $\alpha$ ,  $\beta$ ,  $\rho_1$ ,  $\rho_2$

	$\beta$ [°]	$\alpha$ [°]	$\rho_1$ [mm]	$\rho_2$ [mm]	$A_z$ [mm <sup>2</sup> ]
1	15	7	120	2000	0.18
2	15	7	40	800	0.46
3	15	23	40	2000	0.09
4	0	23	120	800	0.12
5	15	23	120	800	0.07
6	0	7	120	2000	0.28
7	0	23	40	2000	0.10
8	0	7	40	800	0.21

Table 6. Significance coefficient of tested variables

	$\beta$ [°]	$\alpha$ [°]	$\rho_1$ [mm]	$\rho_2$ [mm]
$a_i$	0.0113	-0.0938	-0.0488	-0.0388

Table 7. Results of the calculations included in the test plan and an assessment of the significance of the tested variable

Test variance $S_y^2$	0.00029
Standard deviation $S_y$	0.0171
Number of degrees of freedom $f$	7
Value of $t$ -Student coefficient $t_{(v,f)}$	2.365

Critical value of coefficient $a_{kr}$	0.0406
Significance assessment $ a_i  > a_{kr}$	
$\beta$ [°]	Insignificant
$\alpha$ [°]	Significant
$\rho_1$ [mm]	Significant
$\rho_2$ [mm]	Insignificant

On the basis of the results obtained from the machining simulations and the calculations included in the test plan, it was found that just as in the case of convex-concave surfaces the intersection of the machining layer in the concave-convex surfaces is influenced by the angle of curvature  $\alpha$  and the radius of curvature  $\rho_1$ .

The influence of the lead angle  $\alpha$  and the radius of curvature  $\rho_1$  on the total cross-sectional area of the cutting layer  $A_z$  is shown in Fig. 10.

It is clear from the graph that, as in the simulation of convex-convex surface machining, in this case, the cross-sectional area of the cutting layer  $A_z$  is much more affected by the lead angle  $\alpha$  of the curvature than the radius of curvature  $\rho_1$ . An increase of the lead angle  $\alpha$  from 7° to 23° reduced the cross-sectional area of the  $A_z$  cut by about 50% for a surface whose radius in the feed direction  $\rho_1=40$  mm and by 55% for the contour radius  $\rho_1=120$  mm. An increase of the radius of curvature  $\rho_1$  from 40 mm to 120 mm resulted in an increase in the cross sectional area of the cut layer by about 25% for the lead angle  $\alpha=7^\circ$  and by about 20% for the lead angle  $\alpha=23^\circ$ .

As it is clear from the calculations covered by the test plan, the influence of the angle  $\beta$  and the radius of curvature  $\rho_2$  on the total cross-sectional area of the cut  $A_z$  layer is insignificant. Hence, further research can simplify the concave-convex surface to the concave surface.

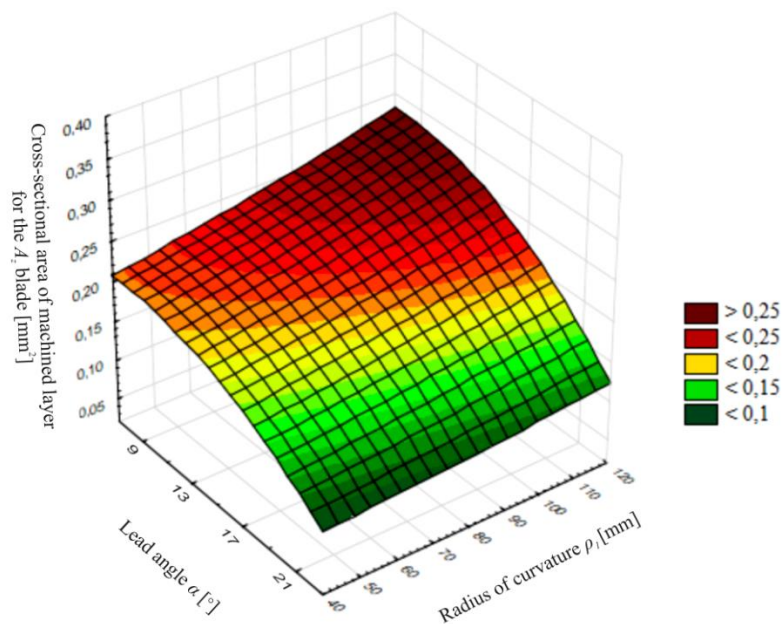


Fig. 10. The effect of the lead angle  $\alpha$  and the radius of curvature  $\rho_1$  on the total cross-sectional area of the sliced  $A_z$  in concave-convex surface machining

Based on the results of the simulation tests it was found that the intersection of the cutting layer in the 5-axis milling process of the surface composed of a toroidal cutter can be significantly influenced by the kinematic parameter of the lead angle  $\alpha$ .

Taking into account the results and the conclusions of the simulated tests, in order to determine the model dependence of the variable radius of curvature  $\rho_1$  and the angle of the lead angle  $\alpha$  on the value of the cutting forces in the range of the tested variables, the machining of the convex and concave surfaces of the turbine blade was adopted.

## 4. EXPERIMENTAL TESTS

### 4.1. STRUCTURE OF THE MODEL TEST OBJECT

The structure of the model of the experimental research object is presented in Fig. 11, while the characteristics of the research object are presented in Table 8.

The input variables of the test object, i.e. the angle  $\alpha$  and the curvature radius- $\rho_1$  as well as the limitations for carrying out experimental tests were selected after taking into account the conclusions of the simulations.

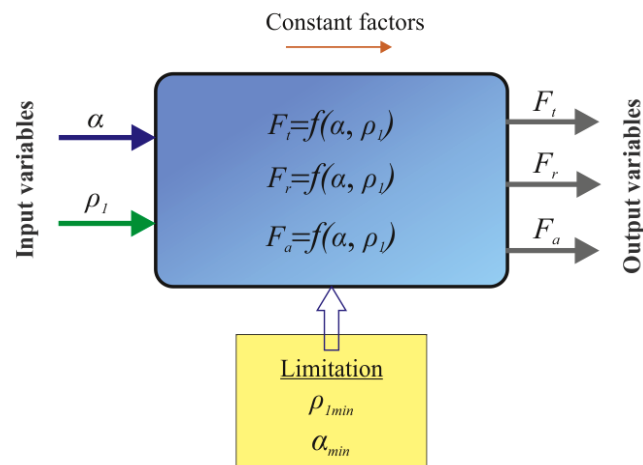


Fig. 11. Structure of the test object

Table 8. Dimensions characteristic for the test object

	Description	
Input variables	X <sub>1</sub>	Lead angle $\alpha$
	X <sub>2</sub>	Curvature radius $\rho_1$ in feed direction
Output variables	Y <sub>1</sub>	Tangent component $F_t$ of cutting force
	Y <sub>2</sub>	Radial component $F_r$ of cutting force
	Y <sub>3</sub>	Axial component $F_a$ of cutting force

Constant factors	C <sub>1</sub>	Machine tool
	C <sub>2</sub>	Material
	C <sub>3</sub>	Tool
Limitation	O <sub>1</sub>	Minimum lead angle $\alpha_{min}$
	O <sub>2</sub>	Minimum concave radius of curvature $\rho_{1min}$

4.2. OBJECT OF EXPERIMENTAL TESTS

The object of the experimental research was the convex and concave surface of the turbine rotor blade which is shown in Fig. 12. These surfaces were unrolled on solid, longitudinal profiles. The angle of blade twisting  $\gamma=0^\circ$  was also constant. The profile of the blade profile was described by arcs with different radii of curvature  $\rho_1$ . The values of these radii were determined on the basis of the actual geometry of the turbine rotor blade. The concave and convex profile is shown in Fig. 13.

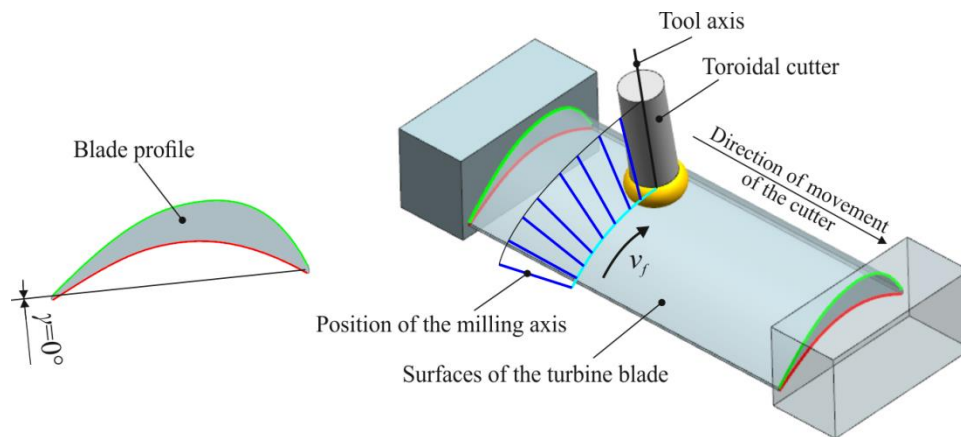


Fig. 12. Test object

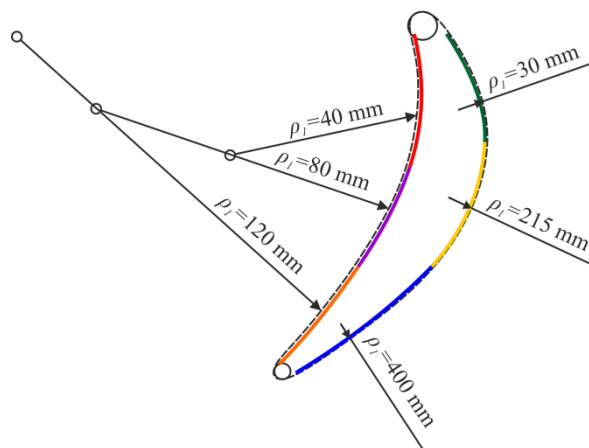


Fig. 13. Convex and concave profile forming blade profile

## 4.3. CONDITIONS OF EXPERIMENTAL TESTS

The convex and concave surfaces were divided into test areas according to the radius of curvature  $\rho_1$  and the angle of rotation  $\alpha$ , as shown in Fig. 14. In contrast, Table 9 shows the machining parameters for convex and concave surface milling.

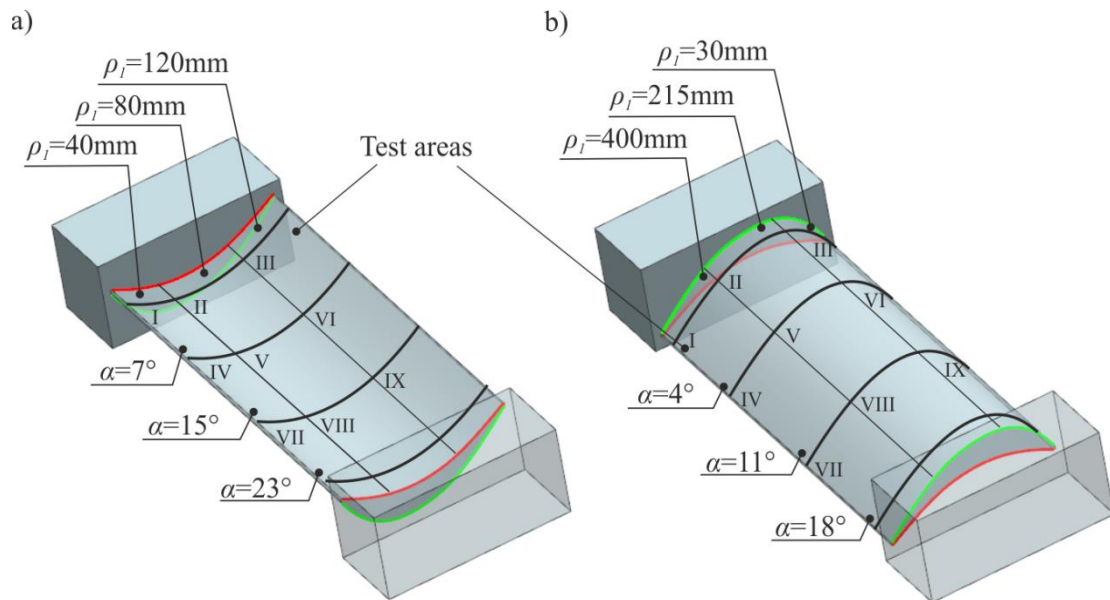


Fig. 14. Test areas depending on the radius of curvature  $\rho_1$  and the lead angle  $\alpha$ :  
a) concave surface, b) convex surface

Table 9. Machining conditions

No.	Parameters	Convex surface machining	Concave surface machining
1.	$a_p$ [mm]	0.25	0.25
2.	$a_e$ [mm]	1.5	1.5
3.	$f_z$ [mm/ostrze]	0.26	0.26
4.	$v_c$ [m/min]	40	40
5.	$\rho_1$ [mm]	$\rho_1 \in <30 \div 400>$	$\rho_1 \in <40 \div 120>$
6.	$\alpha$ [°]	$\alpha \in <4 \div 18>$	$\alpha \in <7 \div 23>$

For each of the processing steps the fixed parameters were: axial infeed  $a_p$ , radial infeed  $a_e$ , blade feed  $f_z$ , toroidal cutter diameter  $D = 16$  mm and the radius of the circular cutting surface  $r_p = 4$  mm. In addition, in order to avoid undercutting of the concave surface, the limit value of the lead angle was calculated  $\alpha_{min} = 7^\circ$  for the radius  $\rho_1 = 40$  mm of this surface.

## 4.4. TEST STATION AND MEASURING TRACK

The test station and track for measuring cutting force components were built on the basis of DMG's 5-axis CNC DMU MonoBlock milling center (Fig. 15), which was provided by the Department of Production Engineering and Automation at the Rzeszow University of Technology. The machine is equipped with NC dividers and tools for roughing and finishing of the test object.

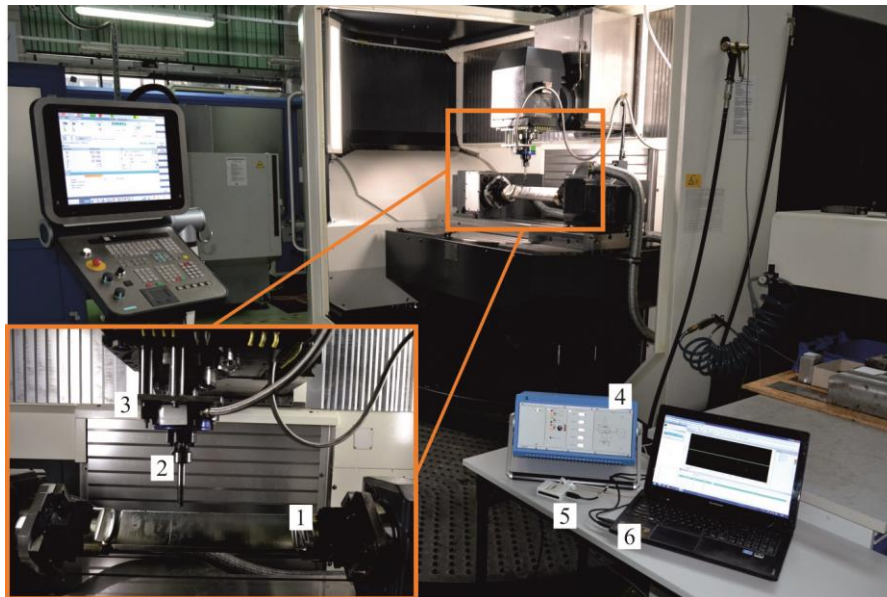


Fig. 15. Measuring track of cutting force components 1 - workpiece, 2 - toroidal cutter, 3 - four piezoelectric rotary force dynamometer, 4 - four-channel signal amplifier, 5 - KUSB KEITHLEY 3100 measurement card, 6 - QuickDAQ software for preview, recording and analysis of measurement signals

A four-piece piezoelectric KISTLER 9123C rotary speed dynamometer was used for measurements. It was mounted in HSK-63A socket of the machine tool spindle that measured forces in the tool system in the following directions:

- X direction ( $F_x$ ) - tangent component measurement  $F_t$ ,
- Y direction ( $F_y$ ) - measurement of radial component  $F_r$ ,
- Z direction ( $F_z$ ) - measurement of the axial component  $F_a$ .

The rotational speedometer's own frequency was  $f_n \approx 2$  kHz.

## 4.5. MATERIALS AND OBJECTS USED FOR TESTING

Experimental tests were carried out on a blade made of Inconel 718 alloy (W. No. 2.4668). This material is a curable nickel-chromium alloy containing also iron, niobium, molybdenum as well as in minor amounts of aluminum and titanium. The Inconel

718 is resistant to corrosion and has high creep resistance at temperatures up to 700°C. This material is used, inter alia, in gas turbine blades, rocket engines, nuclear reactors, pumps, and tooling for machine tools.

The R300-016B20L-08L Sandvik Coromant toroidal milling cutters of diameter  $D = 16$  mm were used for the tests, with R300-0828E-PL circular cutting inserts with the radius  $r_p=4$  mm (Fig. 16).



Fig. 16. Toroidal cutter used for testing

The cutting inserts were made of S30T carbide, especially dedicated to Inconel 718 alloy processing. It is a grade of fine carbide coated with a PVD coating. This carbide is resistant to fatigue wear and micro cracks.

#### 4.6. EXPERIMENTAL TESTS PLAN

Experimental research was conducted in two stages. In the first stage the process of indexing coarse surface of the blade was realized. Roughing was not analyzed and was designed to shape the subject of the research with the assumed finishing allowance. In the second stage the finishing process was realized.

Experimental studies were carried out using a three-level complete PS/DK  $3^n$ , static plan, with the number of repetitions  $r = 3$  and the assumed significance level  $\tau = 0,05$ . This plan allows to obtain the mathematical model of the investigated process in the form of a polynomial function convenient for mathematical analysis and model tests [1]. Table 10 shows the values of the lead angle parameters  $\alpha$  and the radius of curvature  $\rho_1$  for the individual test systems.

Table 10. Test plan for convex and concave surfaces

Test no.	Convex surface		Concave surface	
	$\alpha$ [°]	$\rho_1$ [mm]	$\alpha$ [°]	$\rho_1$ [mm]
1	18	400	23	120
2	18	215	23	80

3	18	30	23	40
4	11	400	15	120
5	11	215	15	80
6	11	30	15	40
7	4	400	7	120
8	4	215	7	80
9	4	30	7	40

4.7. RESULTS OF EXPERIMENTAL TESTS

4.7.1. COMPONENT  $F_t$  OF THE CUTTING FORCE IN THE CONVEX AND CONCAVE SURFACES MACHINING

For the recorded values of the tangent component  $F_t$  of the cutting force the calculations were made according to the accepted test plan. As a result of the calculations the functions of the test object were presented, showing the course of  $F_t$  in the convex surface machining (6) and in the machining of the concave surface (7) in the assumed range of tested parameters  $\rho_1$  and  $\alpha$ :

$$F_t = 412,46 - 28,53\alpha + 0,14\rho_1 + 1,1\alpha^2 - 0,00006\rho_1^2 - 0,0025\alpha\rho_1 \tag{6}$$

$$F_t = 114,05 + 5,95\alpha + 2,5\rho_1 - 0,23\alpha^2 - 0,01\rho_1^2 \tag{7}$$

Based on the obtained functions of the test object, the graphs showing the influence of the curvature radius  $\rho_1$  and the lead angle  $\alpha$  on the tangential component of the cutting force  $F_t$  in the convex surface machining (Fig. 17 ÷ 20) were developed.

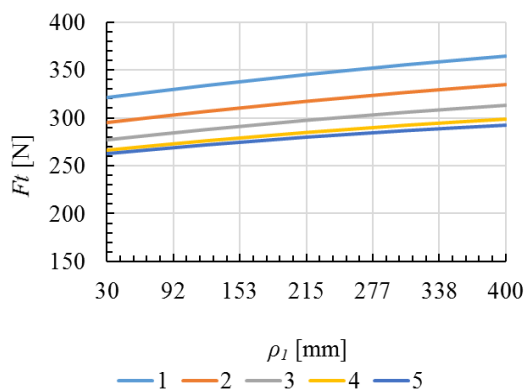


Fig. 17. Influence of the curvature radius  $\rho_1$  on the tangent component  $F_t$  of the cutting force in the convex surface machining: 1)  $\alpha=4^\circ$ , 2)  $\alpha=7,5^\circ$ , 3)  $\alpha=11^\circ$ , 4)  $\alpha=14,5^\circ$ , 5)  $\alpha=18^\circ$

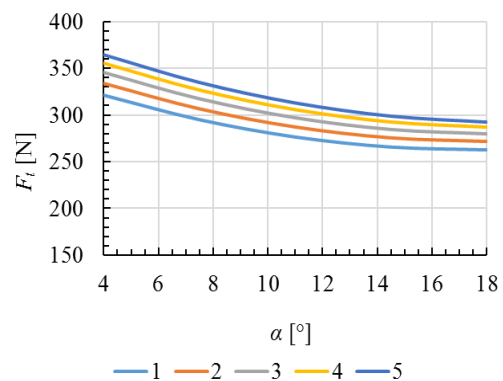


Fig. 18. Influence of the lead angle  $\alpha$  on the tangential component  $F_t$  of the cutting force in the convex surface machining: 1)  $\rho_1=30$  mm, 2)  $\rho_1=122,5$  mm, 3)  $\rho_1=215$  mm, 4)  $\rho_1=307,5$  mm, 5)  $\rho_1=400$  mm

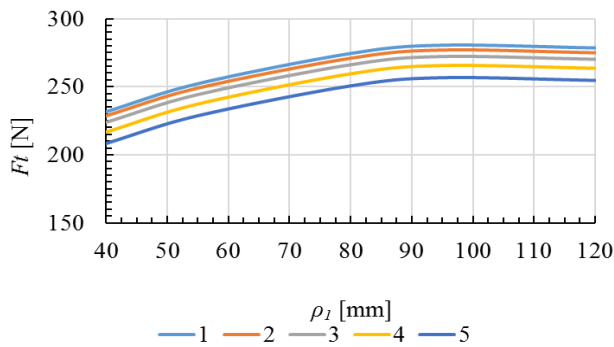


Fig. 19. Influence of the curvature radius  $\rho_1$  on the tangent component  $F_t$  of the cutting force in the convex surface machining: 1)  $\alpha=4^\circ$ , 2)  $\alpha=7,5^\circ$ , 3)  $\alpha=11^\circ$ , 4)  $\alpha=14,5^\circ$ , 5)  $\alpha=18^\circ$

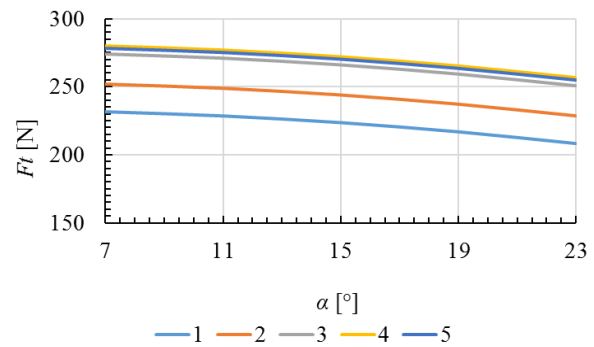


Fig. 20. Influence of the lead angle  $\alpha$  on the tangential component  $F_t$  of the cutting force in the convex surface machining: 1)  $\rho_1=30$  mm, 2)  $\rho_1=122,5$  mm, 3)  $\rho_1=215$  mm, 4)  $\rho_1=307,5$  mm, 5)  $\rho_1=400$  mm

Based on the graphs it was found that in the whole range of curvature radii  $\rho_1$  of the convex and concave surfaces, the value of the component  $F_t$  of the cutting force increases with the increase of the radius of curvature  $\rho_1$ . This is due to the increase in the cross-sectional area value of the cut layer. It was observed that as the miter axis inclination increases in the feed direction, the value of the tangential component  $F_t$  decreases. This is due to changes in the tool contact area with the machined surface and the reduction of the cross-sectional area of the cutting layer.

By comparing the obtained courses it was observed that higher surface values of  $F_t$  were obtained in the machining of the convex surface than in the machining of the concave surface. This is due to the counter-rotating milling that occurs in the convex surface machining due to the positive curvature of the workpiece.

#### 4.7.2. COMPONENT $F_r$ OF THE CUTTING FORCE IN THE CONVEX AND CONCAVE SURFACES MACHINING

For radial component  $F_r$  values of the cutting force, calculations were made according to the accepted test plan. As a result of the calculations, functions of the test object were presented, showing the course of the  $F_r$  in the machining of the convex surface (8) and in the machining of the concave surface (9) in the assumed range of tested parameters  $\rho_1$  and  $\alpha$ :

$$F_r = 93,89 + 0,58\alpha + 0,045\rho_1 - 0,00087\alpha\rho_1 \quad (8)$$

$$F_r = 227,84 - 14,135\alpha + 0,115\rho_1 + 0,42\alpha^2 - 0,00175\rho_1^2 \quad (9)$$

Figures 21 and 22 show graphs based on the relation (7) illustrating the influence of radius of curvature  $\rho_1$  and the lead angle  $\alpha$  on the course of the radial component  $F_r$  of the cutting force measured during the machining of the convex surface. Figures 23 and 24 show graphs based on the relation (8) showing the influence of the parameters  $\rho_1$  and  $\alpha$  on the course of the component  $F_r$  of the cutting force when machining the concave surface.

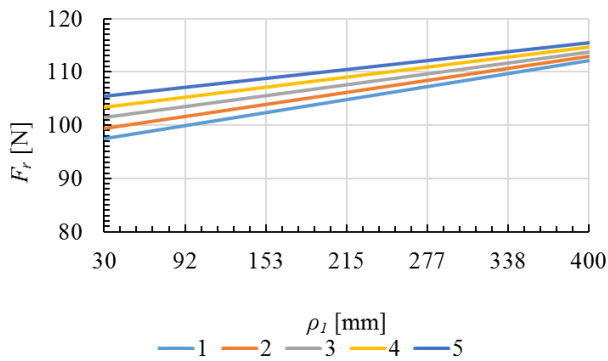


Fig. 21. Influence of the radius of curvature  $\rho_1$  on the radial component  $F_r$  of the cutting force in the surface machining of the convex surface: 1)  $\alpha=4^\circ$ , 2)  $\alpha=7,5^\circ$ , 3)  $\alpha=11^\circ$ , 4)  $\alpha=14,5^\circ$ , 5)  $\alpha=18^\circ$

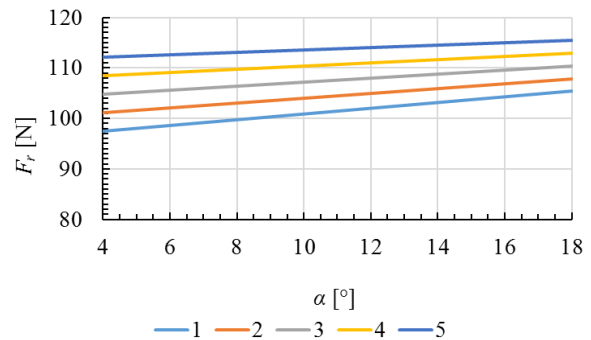


Fig. 22. Influence of the lead angle  $\alpha$  on the radial component  $F_r$  of the cutting force on the surface machining of the convex surface: 1)  $\rho_1=30$  mm, 2)  $\rho_1=122,5$  mm, 3)  $\rho_1=215$  mm, 4)  $\rho_1=307,5$  mm, 5)  $\rho_1=400$  mm

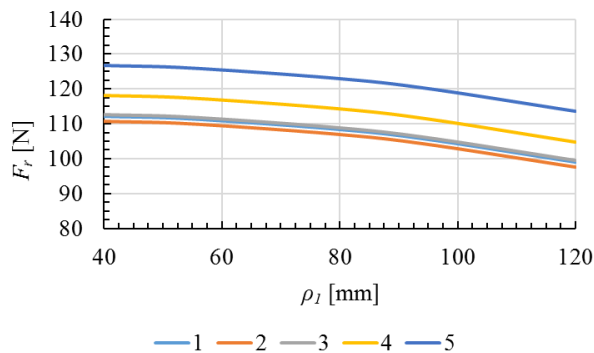


Fig. 23. Influence of the radius of curvature  $\rho_1$  on the radial component  $F_r$  of the cutting force in the surface machining of the convex surface: 1)  $\alpha=4^\circ$ , 2)  $\alpha=7,5^\circ$ , 3)  $\alpha=11^\circ$ , 4)  $\alpha=14,5^\circ$ , 5)  $\alpha=18^\circ$

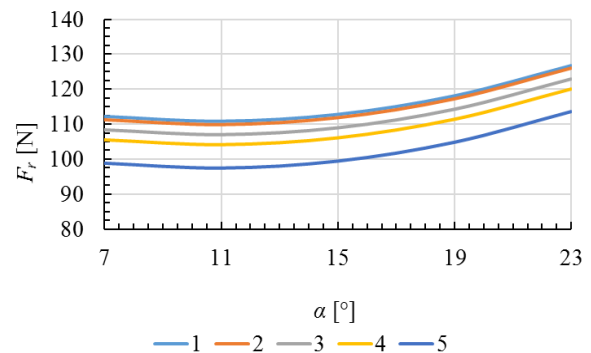


Fig. 24. Influence of the lead angle  $\alpha$  on the radial component  $F_r$  of the cutting force on the surface machining of the convex surface: 1)  $\rho_1=30$  mm, 2)  $\rho_1=122,5$  mm, 3)  $\rho_1=215$  mm, 4)  $\rho_1=307,5$  mm, 5)  $\rho_1=400$  mm

The graphs show that in all assumed range an increase in parameter  $\rho_1$  in the convex surface machining makes that the value  $F_r$  also increases, whereas in the case of a concave surface it decreases. A growth of  $F_r$  for the convex surface can be explained by the extension of the cutter contact line with the contour of the machined surface and the increase in the angle of lap of the cutter. With an increase of the cutter axis inclination in the feed direction, the value of the radial component  $F_r$  of the cutting force grows in the machining of both surfaces. This is due to the change of the point and contact area of the cutter to the machined surface, and thus to the increase in the cross-sectional area of the cut.

When comparing the received courses of the radial component  $F_r$  of the cutting force it was observed that the increment of the radial component  $F_r$  of the cutting force in the machining of the convex surface results mainly from the increase in the radius of curvature  $\rho_1$ , while in the machining of the concave surface from the increase in the value of the lead angle  $\alpha$ .

#### 4.7.3. COMPONENT $F_a$ OF THE CUTTING FORCE IN THE CONVEX AND CONCAVE SURFACES MACHINING

For the recorded values of the axial component  $F_a$  of the cutting force calculations were made according to the adopted test plan. As a result of the calculations one obtained the functions of the test object showing the course of  $F_a$  in the machining of the convex surface (10) and in the machining of the concave surface (11) in the assumed range of tested parameters  $\rho_1$  and  $\alpha$ :

$$F_a = 281,62 + 10,81\alpha + 0,156\rho_1 + 0,23\alpha^2 - 0,005\alpha\rho_1 \quad (10)$$

$$F_a = 331,35 - 7,145\alpha - 0,16\rho_1 + 0,26\alpha^2 + 0,01\alpha\rho_1 \quad (11)$$

The graphs created on the basis of the obtained functions of the test object show the influence of the curvature radius  $\rho_1$  of the convex surface and the lead angle  $\alpha$  on the course of the axial component  $F_a$  of the cutting force. They are shown in Fig. 25 and 26. In Fig. 27 and 28 there are graphs that show the influence of radius of curvature  $\rho_1$  and the lead angle  $\alpha$  in the machining of the concave surface on the course of this force.

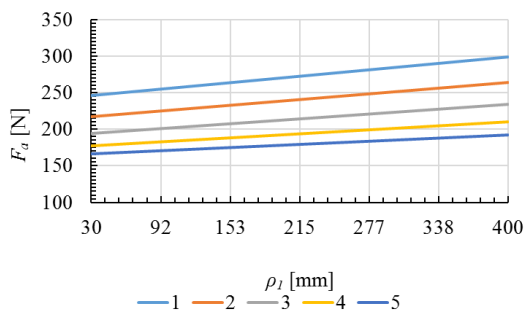


Fig. 25. Influence of the radius of curvature  $\rho_1$  on the axial component  $F_a$  of the cutting force on the convex surface machining: 1)  $\alpha=4^\circ$ , 2)  $\alpha=7,5^\circ$ , 3)  $\alpha=11^\circ$ , 4)  $\alpha=14,5^\circ$ , 5)  $\alpha=18^\circ$

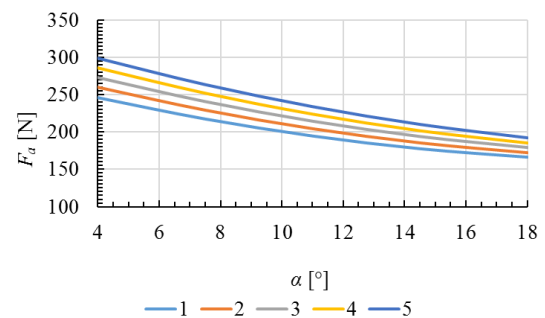


Fig. 26. Influence of the lead angle  $\alpha$  on the axial component  $F_a$  of the cutting force in the convex surface machining: 1)  $\rho_1=30$  mm, 2)  $\rho_1=122,5$  mm, 3)  $\rho_1=215$  mm, 4)  $\rho_1=307,5$  mm, 5)  $\rho_1=400$  mm

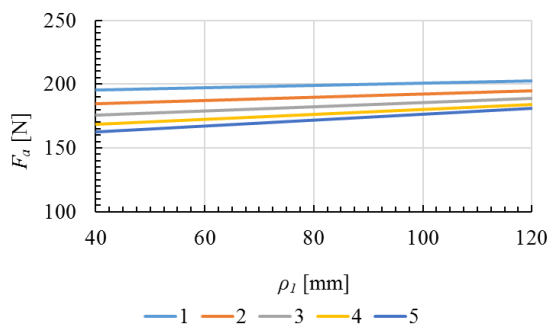


Fig. 27. Influence of the radius of curvature  $\rho_1$  on the axial component  $F_a$  of the cutting force on the concave surface machining: 1)  $\alpha=4^\circ$ , 2)  $\alpha=7,5^\circ$ , 3)  $\alpha=11^\circ$ , 4)  $\alpha=14,5^\circ$ , 5)  $\alpha=18^\circ$

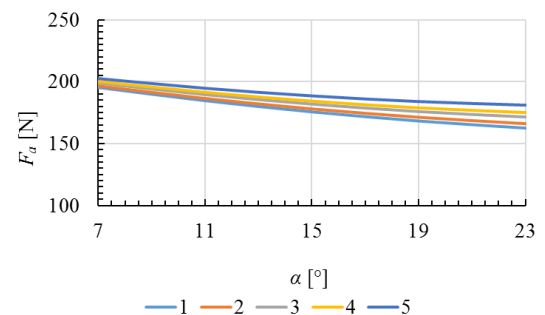


Fig. 28. Influence of the lead angle  $\alpha$  on the axial component  $F_a$  of the cutting force in the concave surface machining: 1)  $\rho_1=30$  mm, 2)  $\rho_1=122,5$  mm, 3)  $\rho_1=215$  mm, 4)  $\rho_1=307,5$  mm, 5)  $\rho_1=400$  mm

The graphs show that the value of the axial component  $F_a$  of the cutting force increases with a growth of the radius of curvature  $\rho_1$ . On the other hand, an increase in the lead angle  $\alpha$  of the cutter axis causes the reduction of the axial component  $F_a$  of the cutting force in the machining of both surfaces. When comparing the received courses of the axial component  $F_a$  of the cutting force as a function of the lead angle  $\alpha$  and the radius of curvature  $\rho_1$  it was also found that in machining of the convex surface the values of axial component  $F_a$  of the cutting force was greater than in the machining of the concave surface. This is the result of the conventional cut milling that occurs in the milling of the convex surface.

## 5. SUMMARY

The simulation of the 5-axis milling process with toroidal cutters and the assessment of the influence of the lead angle  $\alpha$ , the angle of inclination  $\beta$  and the radius of curvature  $\rho_1$  in the direction of feed and radius of curvature  $\rho_2$  in the direction perpendicular to the feed it was found that the intersection of the cut layer in the convex-concave and concave-convex machining was only influenced by the lead angle  $\alpha$  and the radius of curvature  $\rho_1$  in the tool feed direction.

On the basis of the experimental studies and the analysis of the obtained results of the cutting forces, it can be stated that with an increase of the radius of curvature  $\rho_1$  within the range tested, the contact area between the tool and the treated surface, both convex and concave, increases as well. Consequently, this results in an increase in the component cutting forces. This fact results from the fact that with an increasing contact zone, the cross section of the cutting layer increases, resulting in increasing values of the cutting forces. On the other hand, with an increase in the lead angle  $\alpha$ , the contact zone decreases. This results in a decrease in the cutting section's cross-sectional value and thus in the cutting force values. The exception is the radial component  $F_r$  of the cutting force, whose value slightly increases with an increase of the lead angle  $\alpha$ .

It was also found that the machined surfaces of the convex and concave surface generated during the machining process can be significantly influenced by the kinematic parameter of the lead angle  $\alpha$ . It can be assumed that this parameter can also indirectly influence the deviation of the  $\Delta_k$  shape as well as the surface roughness parameters, but confirmation of this requires further investigation in this direction.

In summarizing the above conclusions, it can be stated that the values of the lead angle  $\alpha$  in the surface machining of the convex and concave turbine blade should be varied continuously with the radius of curvature  $\rho_1$  of the machined surface profile.

## REFERENCES

- [1] ZHANG X., YU T., WANG W., 2014, *Modeling, simulation, and optimization of five-axis milling processes*, The International Journal of Advanced Manufacturing Technology, 74/9-12, 1611-1624.
- [2] FUSSELL B.K., JERARD R.B., HEMMETT J.G., 2003, *Modeling of cutting geometry and forces for 5-axis sculptured surface machining*, Computer-Aided Design, 35, 333-346.

- [3] BAILEY T., ELBESTAWI M.A, EL-WARDANY T.I., FITZPATRICK P., 2002, *Generic simulation approach for multi-axis machining, Part 1: Modeling methodology*, Journal of Manufacturing Science and Engineering, 124, 624-633.
- [4] BUDAK E., OZTURK E., TUNC L.T., 2009, *Modeling and simulation of 5-axis milling processes*, CIRP Annals-Manufacturing Technology, 58/1, 347-350.
- [5] KAWALEC A., MAGDZIAK M., 2017, *The selection of radius correction method in the case of coordinate measurements applicable for turbine blades*, Precision Engineering, 49, 243-252.
- [6] MAGDZIAK M., 2017, *The influence of a number of points on results of measurements of a turbine blade*, Aircraft Engineering and Aerospace Technology, 89/6, 953-959.
- [7] ERDIM H., LAZOGLU I., OZTURK B., 2006, *Feedrate scheduling strategies for free-form surfaces*, International Journal of Machine Tools and Manufacture, 46, 747-757.
- [8] ERDIM H., LAZOGLU I., KAYMAKCI M., 2007, *Free-form surface machining and comparing feedrate scheduling strategies*, Machining Science and Technology, 11, 117-133.
- [9] FERRRY W.B., ALTINTAS Y., 2008, *Virtual five-axis flank milling of jet engine impellers – Part I: Mechanics of five-axis flank milling*, Journal of Manufacturing Science and Engineering, 130, 51-61.
- [10] GDULA M., BUREK J., ŻYŁKA Ł., 2014, *Cross section of the cutting layer in simultaneous five-axis machining of sculptured surfaces*, Archives of Mechanical Technology and Automation, 34/4, 25-36.
- [11] GDULA M., BUREK J., ŻYŁKA Ł., TUREK P., 2014, *Analysis of accuracy of the shape of sculptured surfaces in simultaneous five-axis machining of parts made from difficult to machine materials used in aviation technology*, Archives of Mechanical Technology and Automation, 34/4, 11-24.
- [12] OZTURK E., BUDAK E., 2007, *Modeling of 5-axis milling processes*, Machining Science and Technology: An International Journal, 11, 287-311.
- [13] DAVIM J.P., 2012, *Machining of complex sculptured surfaces*, Springer-Verlag, London.
- [14] RADZEVICH P.S., 2014, *Generation of surface machining*. CRC Press Taylor and Francis Group, New York.
- [15] GILLES P., COHEN G., MONIES F., 2013, *Torus cutter positioning in five-axis milling using balance of the transversal cutting force*, International Journal Advanced Manufacturing Technology, 66, 965-973.
- [16] MAGDZIAK M., 2016, *An algorithm of form deviation calculation in coordinate measurements of free-form surfaces of products*, Strojniški vestnik - Journal of Mechanical Engineering, 1/62, 51-59.
- [17] ALTMÜLER S., 2001, *Simultanes fünfachsiges Fräsen von Freiformflächen aus Titan*, Doctoral Dissertation, Aachen.
- [18] GDULA M., 2017, *Process of simultaneous five-axis milling of sculptured surfaces of the toroidal cutter*, Doctoral Dissertation, Rzeszów.
- [19] OZTURK E., TUNC T., BUDAK E., 2009, *Investigation of lead and tilt angle effects in 5-axis ball-end milling processes*, International Journal of Machine Tools and Manufacture, 49/14, 1053-1062.
- [20] HENDRIKO H., KISWANTO G., ISTIYANTO J., DUC E., 2017, *Implementation of analytical boundary simulation method for cutting force prediction model in five-axis milling*, Machining Science and Technology: An International Journal, 1-17.
- [21] SADILEK M., CEP R., BUDAK I., SOKOVIC M., 2011, *Aspects of using tool axis inclination angle*, Journal of Mechanical Engineering, 57, 681-688.